Hindawi
International Journal of Aerospace Engineering
Volume 2021, Article ID 8883194, 10 pages
https://doi.org/10.1155/2021/8883194

Research Article

Experimental Investigation on Flow Field Characteristics of Impinging-Film Cooling

Jingyu Zhang, Ping Jiang, Ce Yuan, and Xiaomin He

College of Energy and Power Engineering, Nanjing University of Aeronautics and Astronautics, Nanjing 210016, China

Correspondence should be addressed to Jingyu Zhang; zjyhxm@nuaa.edu.cn

Received 16 September 2020; Revised 6 November 2020; Accepted 24 November 2020; Published 4 January 2021

Academic Editor: Dakun Sun

This paper describes an experimental investigation on flow field characteristics of impinging-film cooling. Particle Image Velocimetry (PIV) technology has been applied to observe the effect of blowing ratio ($0.04 \le M \le 0.3$), temperature ratio ($0.73 \le T_u \le 0.91$), jet-to-plate pitch ($1.6 \le Z_n \le 3.2$), and spacing of impinging holes ($1.94 \le Y_n \le 3.5$) on the flow field patterns in an impinging-film cooling test rig under atmospheric pressure. Experiment results show that the near-wall entrained vortex at the downstream of the slit moves downstream of the test rig as the blowing ratio increases, which increases the effective protection length of the film. While the vortex at the end of the inducting slab is stronger, this will increase the mixing in the shear layer. The radial size of the near-wall entrained vortex tends to decrease as the temperature ratio increases at the low blow ratio, and the entrainment effect on the downstream of the slit becomes smaller, causing the separation zone to decrease. Increasing the jet-to-plate pitch, the size of the near-wall entrained vortex increases, and the thickness of the film layer increases, this strengthens the separation effect of the near-wall airflow from the wall surface. The larger the spacing of the impinging holes, the more uneven the velocity distribution of the film.

1. Introduction

To meet the requirements of high-performance, high thrust-to-weight ratio aircrafts, aeroengines are developing in the direction of the high compressor pressure ratio and high temperature rise [1]. Increasing the compressor pressure ratio will increase the inlet temperature of the combustor, which means that the temperature of the cooling air in the liner will increase, causing its cooling effectiveness to decrease rapidly. To increase the temperature rise of the combustor, it is necessary to increase the fuel to the air ratio of the combustor to increase the outlet temperature, and then the proportion of air required for combustion is increasing. With the increase of the outlet temperature, more air in the combustor will be distributed in the mixing zone for regulating the outlet temperature field to protect the life of the turbine. This makes the amount of air used for liner cooling less and less. Increasing the temperature rise of the combustion will also increase the thermal radiation of the hot products to the liner, which will increase the temperature of the liner [2]. However, the amount of air used for cooling has been continuously reduced, and the cooling quality of the cooling air has decreased. This has made the problem of liner cooling more and more prominent and has also brought new challenges to the technology of liner cooling. Therefore, it is very important to choose the proper liner cooling technology and develop efficient cooling technology to ensure the combustion performance and combustor life.

At present, the cooling technologies applied in aeroengines are mainly including film cooling [3–5], transpiration cooling [6–8], and impinging-film cooling [9–11]. Film cooling is the most commonly used for liner cooling. Film is used to cool and isolate the hot products from scouring the wall. When the outlet temperature of the combustor is less than 1600 K, the cooling air volume of the film cooling can be more than 40% [12]. However, with the further increase of the outlet temperature, film cooling is no longer suitable for high temperature rise combustors. Transpiration cooling is a type of cooling technology that makes full use of the heat transfer process of the divergent hole to improve the cooling capacity of the cooling air and reduce the air consumption at the same time [13]. However, the diameter of the

transpiration cooling hole is too small, which is easy to be blocked by soot and corrosion by hot products. This is easy to reduce the cooling effect, and the performance is not reliable. Impinging-film cooling is an efficient hybrid cooling technology suitable for working conditions with high pressure drop of the combustor. It can make full use of the pressure drop of the liner and use the impinging flow to improve the cold-side heat transfer capacity. Among various types of cooling technologies, the impinging-air film cooling has the following advantages [10, 11, 14–17]: (1) the cooling efficiency is high, the formed film is more uniform, and the circumferential temperature gradient on the wall surface is small; (2) the cooling structure is simple and easy to process; and (3) the proportion of cooling air is small, between 25% and 30%. Therefore, the impinging-air film cooling has a good application prospect on high temperature rise combustors.

The heat transfer model of the impinging-air film cooling structure is shown in Figure 1. There are five main heat transfer processes including the radiation of hot products to the liner, the radiation of the liner to the casing, and the heat convection of the hot and cold sides of the liner and heat conduction inside the liner. The amount of heat exchange in each part is related to many other factors such as the structure of the flow field of the impinging-air film cooling, the temperature and the composition of the hot products, and the concentration of particles in the hot products.

In the impinging-air film structure with an inducting slab, cooling air is ejected from the jet hole, and the inducting slab is cooled. Then, the jets merge in the impinging cavity formed by the inducting slab and the liner and flow out from the slit outlet. A layer of film is formed on the downstream wall to protect the liner. The velocity distribution of an ideal two-dimensional film is shown in Figure 2 [11]. It can be mainly divided into three parts: boundary layer, core area, and shear layer. The boundary layer and the core area isolate the hot products and protect the liner. The shear layer is the mixing area of cooling air and hot products. The lower the mixing degree in the shear layer, the longer the effective protection length of the film and the better the cooling effect. The film in the combustor is greatly different from the ideal film due to the influence of liner wall roughness, turbulence, radiation, and other factors. This has caused the flow and heat transfer mechanism of the impinging-air film to become more complicated, and it has also gained more and more attention from researchers.

Jia [18] studied the effects of jet inclination on the flow field and adiabatic temperature ratio of the slit air film through numerical simulation and experimental methods. The results show that when the jet inclination is greater than 40°, a significant recirculation zone will be formed downstream the slit. When the angle is less than 30°, the recirculation zone will disappear; when the jet angle is 30°, the slit air film has the highest adiabatic temperature ratio. Wang [19] studied the flow mixing characteristics of discrete-hole and slit-type film experimentally. In the experiment, a five-hole probe was used to measure the velocity and pressure distribution in the slit, and the effects of the azimuth of the hole, the tilt angle of the slit, the length and width of the slit on the uniformity of the velocity distribution of the slit, and the total pressure loss of the flow were studied. Studies have shown that when the azimuth of the hole is 60° and the inclination of the slit is 30°, the airflow velocity uniformity at the exit of the slit is the best, and the total pressure loss is small. Cruz [20] studied the mixing characteristics of the primary stream and the secondary stream of the two-dimensional slit air film. In the experiment, three different velocity ratios were set for the primary stream and the secondary stream (VR = 2, VR = 1, and VR = 0.5). It was found that the air film mixing was the least when the velocity ratio was 1. Gogineni [21] studied the effects of turbulence and blowing ratio of film cooling on the flow field downstream of the film hole by PIV technology and analyzed the formation and development of vortices in the flow field. The results show that the inlet turbulence increases, and the thickness of the secondary and mainstream shear layers increases. However, after the blowing ratio exceeds 1.5, the effect of the turbulence on the shear layer decreases. Zhang [11] investigated the effects of blowing ratio, nondimensional jet-to-plate pitch, nondimensional spacing of jet holes, and diameter of jet hole on overall cooling effectiveness of impinging-film cooling. The results show that overall cooling effectiveness invariably increases with a raise in the blowing ratio. The cooling performs better as nondimensional jet-to-plate pitch increases. The decline of nondimensional spacing of jet holes improves the overall cooling effectiveness at higher blowing ratios ($M \geq 0.91$), which was not observed in cases with low blowing ratios ($M \leq 0.61$). The variation of the hole diameter (1.0–1.8 mm) has little influence on the cooling performance. Wei [10] numerically investigated the impinging-film cooling effect with different geometries including cross-sections of the inducting slab (rectangular or triangular), inducting channels (convergent, uniform and divergent), and jet

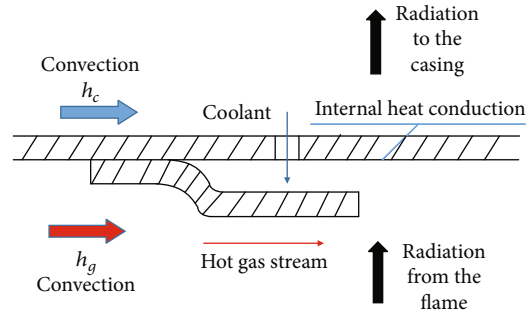

Figure 1: Heat transfer model of combustor wall.

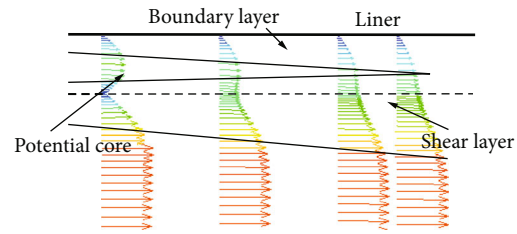

Figure 2: Velocity distribution of simple ideal slot-film cooling.

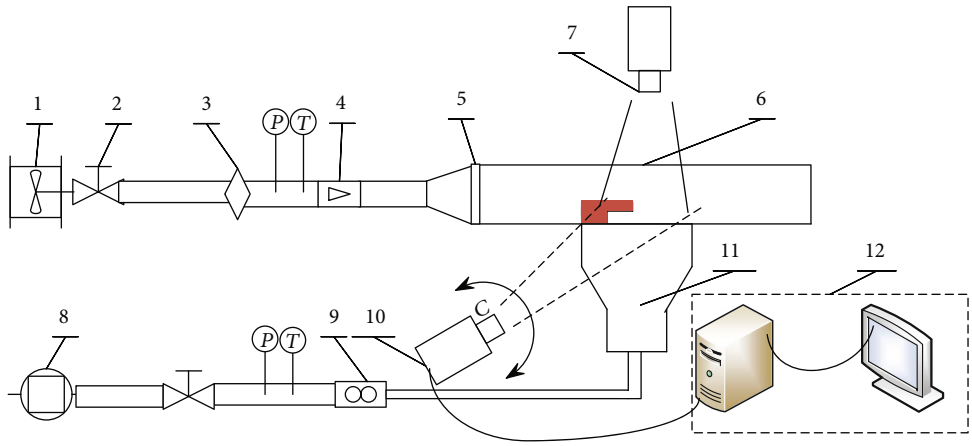

Figure 3: Schematic diagram of the impinging-film cooling experimental system. 1-Single screw compressor; 2-Valve; 3-Electric heater; 4-Vortex flowmeter; 5-Metal grille; 6-Heat airflow chamber; 7-Laser; 8-Piston compressor; 9-Glass rotor flowmeter; 10-CCD camera; 11-Coolant airflow chamber; 12-PIV data processing system.

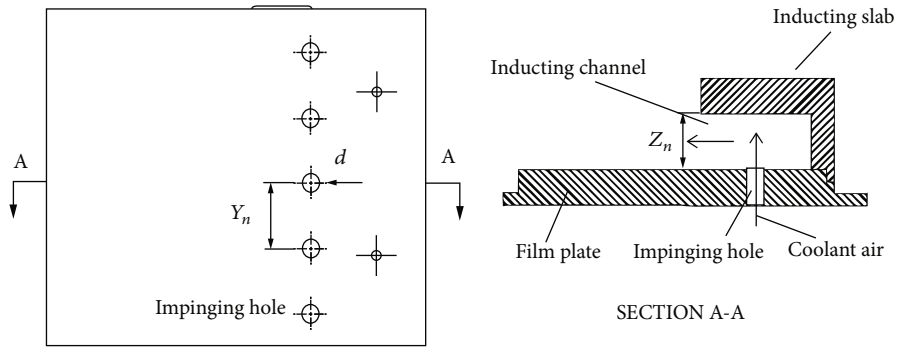

(a) Top view (b) Front view

Figure 4: Schematic structure of an impinging-film cooling test rig.

inclinations (30°, 45°, 60°, and 90°). The results show that the convergent channel can improve by 8.12% on the local cooling effectiveness while divergent one decreases by 16%. The jet inclination is found to have little effect on the cooling effectiveness, but plays an important role on determining the temperature distribution of the surface close to the primary flow of inducting slab. The best performance was obtained with the inclination of 60° considering both liner and inducting slab. Research results on cooling technologies show that cooling efficiency is closely related to the characteristics of the flow field, which are mainly related to the adherence effect of the air flow, the core flow length, the secondary flow and the mainstream mixing characteristics, and the uniformity of the film spreading speed. The important method to improve the cooling efficiency of the film is to optimize the flow field structure by changing the flow and geometric parameters. Therefore, it is very important to study the flow field of the impinging-air film cooling. References [10, 22–26] have studied flow field characteristics through numerical simulation methods, but there are few experimental studies on flow field characteristics, especially for the flow field structure, and the experimental study of shear layer mixing is still scarce.

The scope of this paper is to investigate the flow field characteristics of the impinging-air film cooling using PIV technology. Focus on the study of the effects of different flow parameters including blowing ratio, temperature ratio, jet-to-plate pitch, and spacing of jet holes on the flow field and shear layers mixing characteristics of impinging-air film cooling. This paper lays a theoretical foundation for optimizing the film cooling structure and the flow field control methods.

2. Experimental Setup

The experimental system mainly includes test rig, airflow supply system, PIV measurement system, and measurement system, as shown in Figure 3.

Figure 4 shows the schematic structure of an impinging-film cooling test rig, which is mainly composed of a film plate with a row of impinging holes and an inducting slab. The coolant air impinges against on the inducting slab through the impinging holes and is directed along the inducting channel by the inducting slab and then it jets out and forms a colder film on the film plate. The test rig is made of 45 steel, and the thickness of the film plate and the inducting slab is 15 mm.

Two airflows were supplied in the experiment, namely, the primary airflow and the secondary airflow. The primary airflow was fed by a single screw air compressor with a maximum mass flow rate of 34.4 m^3/min and then heated by an electric heater up to 573.15 K, which is used to simulate the

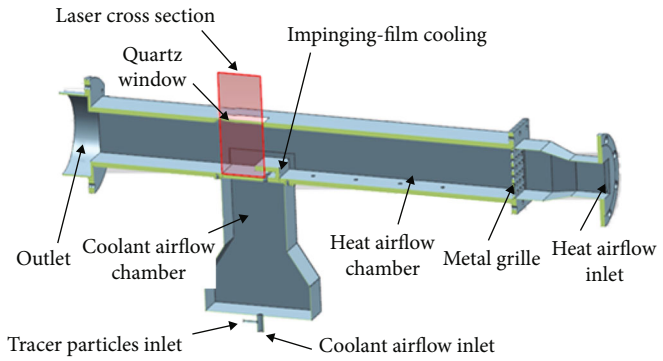

Figure 5: Details of the test section.

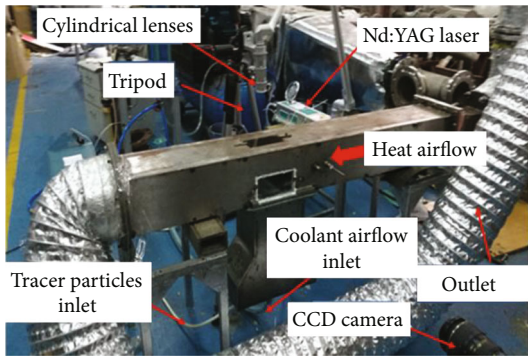

Figure 6: Physical picture of the PIV experimental setup.

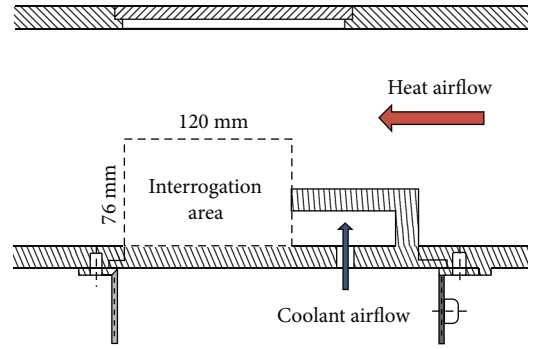

Figure 7: Schematic diagram of the interrogation area in the PIV experiment.

hot gas in the combustor. The secondary airflow is provided by a piston compressor with a maximum mass flow rate of 2 m^3/min at ambient temperature to simulate the cooling air. Both flows were adjusted by supply throttling valve and return flow throttling valve.

The primary airflow enters the experimental section after being rectified by the metal grille, forming an initial cross flow. After being rectified in the cold air cavity, the secondary airflow impinges against on the inducting slab through the impinging holes and then mixing with the primary flow and flows out from the outlet, as shown in Figure 5. To effectively carry out PIV experiments, quartz windows are provided on the upper and side walls of the test section that allowed large optical access for the laser sheet and the camera. The surface of the test rig and the unmeasured area in the test section were blackened to avoid reflections on the wall and effectively improve the PIV measurement accuracy.

Characterization of the nonreacting flow field in the impinging-film cooling test rig was performed by using a high-resolution PIV. The PIV system consisted of a dual-cavity pulsed Nd:YAG laser, a frame-straddling charge-coupled device (CCD) camera, a combination of cylindrical lenses, a seven-joint light guide arm, a laser power, a synchronization circuit, and Micro Vec3.0 postprocessing software computer, as shown in Figure 6.

Hollow microglass beads, with a mean diameter of ~5 μm, bulk density of 0.1~0.7 g/cm^3 and good followability in the airflow, was seeded into the secondary airflow, which ensured that the tracer particles could be well mixed with the flow and uniformly distributed in the PIV measurement. Depending on the impinging-film cooling location and considering the geometrical limitations, the interrogation area was measured through vertical cross-section of the center imping hole, as shown in Figure 7.

All the PIV experiments were conducted under atmospheric pressure. Investigations on the effect of the blowing ratio ($0.04 \le M \le 0.3$), temperature ratio ($0.73 \le T_R \le 0.91$), jet-to-plate pitch ($1.6 \le Z_n \le 3.2$), and spacing of jet holes ($1.94 \le Y_n \le 3.5$) on the flow field patterns in an impinging-film cooling test rig are the primary purpose of the current study. The detailed operational parameters for the combustor are summarized in Table 1.

The blowing ratio (M) is the mass flow ratio between the primary airflow and the secondary airflow and is defined as

$$M = \frac{\rho_s u_s}{\rho_h u_h} = \frac{m_c}{A_s \rho_h u_h} = \frac{A_h \rho_c v_c}{A_s \rho_h v_h}. \quad (1)$$

The temperature ratio (T_R) is the ratio of primary airflow temperature to secondary airflow temperature and is defined as

$$T_R = \frac{T_c}{T_h}. \quad (2)$$

Table 1: Operating Conditions for PIV Experiments.

Blowing ratio M	Temperature ratio T_R	Jet-to-plate pitch Z_n	Spacing of jet holes Y_n
0.04, 0.1, 0.3	0.73, 0.82, 0.91	2.4	3.5
0.04, 0.1, 0.3	0.73	1.6	3.5
0.04, 0.1, 0.3	0.73	3.2	3.5
0.04, 0.1, 0.3	0.73	2.4	2.5
0.04, 0.1, 0.3	0.73	2.4	1.94

Table 2: Uncertainty of flow field experimental measurement parameters.

W_i, units	Value	$\triangle W_i$	$(\triangle W_i/W_i)\%$	Note
T_c, K	308	±0.5	±0.16	Secondary airflow temperature
T_h, K	338.46~423.15	±0.5	±0.15	Primary airflow temperature
P_c, pa	$(1.013 \sim 1.313) \times 105$	±75	±2.5	Secondary airflow pressure
p_H, pa	$(1.013 \sim 1.413) \times 105$	±100	±2.5	Primary airflow pressure
V_h, m^3/h	420	±10.5	±2.5	Primary airflow volume flow rate
V_c, m^3/h	1.7~18.9	±0.47	±2.5	Secondary airflow volume flow rate

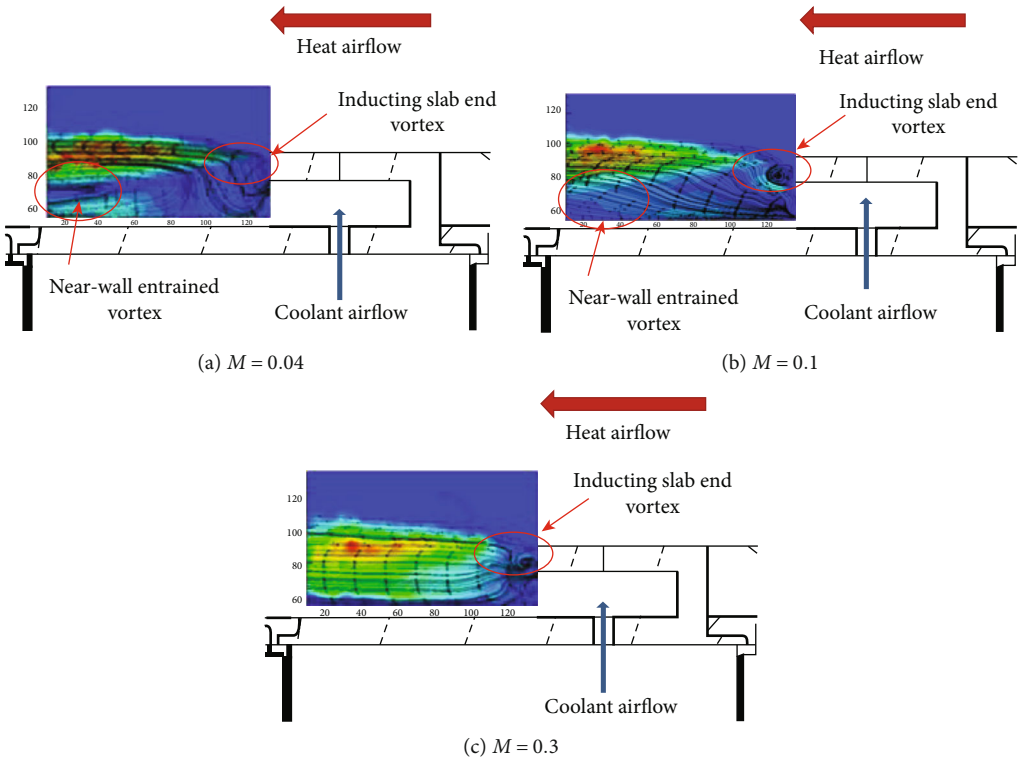

Figure 8: Flow field pattern at different blowing ratios.

The jet-to-plate pitch (Z_n) is the ratio of the distance between the film plate and the inducting slab to the diameter of the impinging hole and is defined as

$$Z_n = \frac{z_n}{d}. \quad (3)$$

The spacing of jet holes (Y_n) is the ratio of the impinging hole spacing to the diameter of the impinging hole and is defined as

$$Y_n = \frac{y_n}{d}. \quad (4)$$

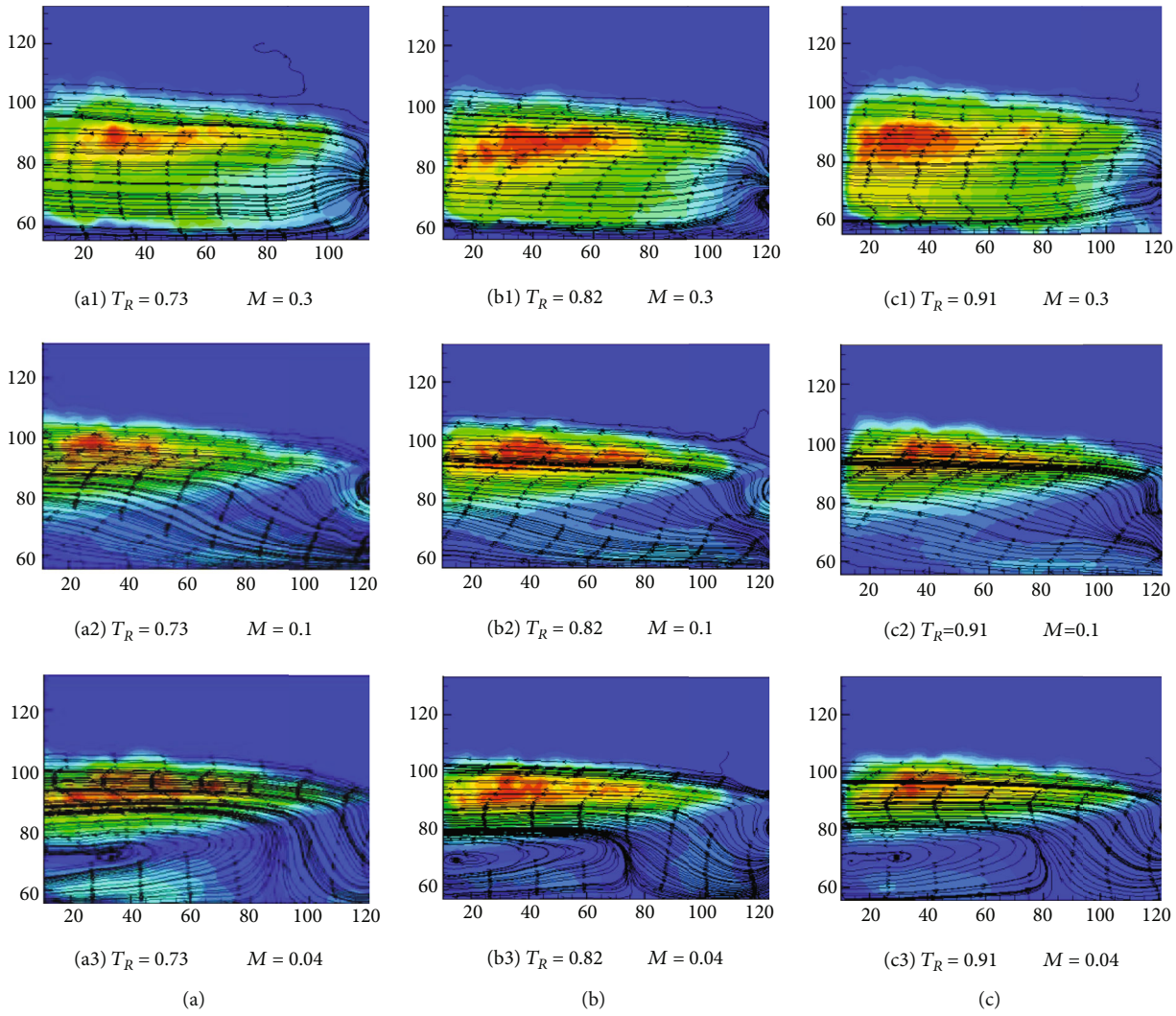

Figure 9: Flow field pattern at different temperature ratios.

The primary airflow mass flow rate is measured by a vortex flowmeter, and the accuracy level is 2.5. The secondary airflow mass flow rate is measured by a glass rotor flowmeter with a precision level of 2.5. Both the temperatures of the airflow are measured by T-type thermocouple, with a thermocouple accuracy rating of 1. The pressure of the airflow is measured by a precision pressure gauge, and the accuracy level is level 1. The uncertainty of the measured parameters of the flow field experiment is shown in Table 2.

3. Results and Discussions

This paper describes an experimental investigation of flow field characteristics of impinging-film cooling using PIV technology. The effect of the blowing ratio, temperature ratio, jet-to-plate pitch, and spacing of impinging holes on the flow field patterns in an impinging-film cooling test rig was observed under atmospheric pressure. Now, the experimental results will be introduced and analyzed in detail.

3.1. Effect of the Blowing Ratio, M. Figure 8 shows how the flow field pattern changes with blowing ratios. Experiments were conducted by fixing the temperature ratio at 0.73, the jet-to-plate pitch at 2.4, and the spacing of impinging hole 3.5. The blowing ratios are then fixed at 0.04, 0.1, and 0.3, respectively. It can be seen from the figure that when the blowing ratio is 0.04, there is an entrained vortex near the wall of the film plate and a small vortex at the end of the inducting slab in the flow field downstream of the slit exit. The reason for the occurrence of entrained vortices is that the mainstream is a subsonic airflow. When passing through the sudden expansion zone, an adverse pressure gradient will be formed, and the airflow at the exit of the slit is not enough to overcome the adverse pressure gradient and causes flow separation there. This result in a large amount of heat flow is drawn into the near wall of the film plate, which is not conducive to cooling the wall. The vortex at the end of the inducting slab is formed because this region is a low-speed region between hot and cold airflows, and there is a large reverse pressure gradient. This vortex is located at the

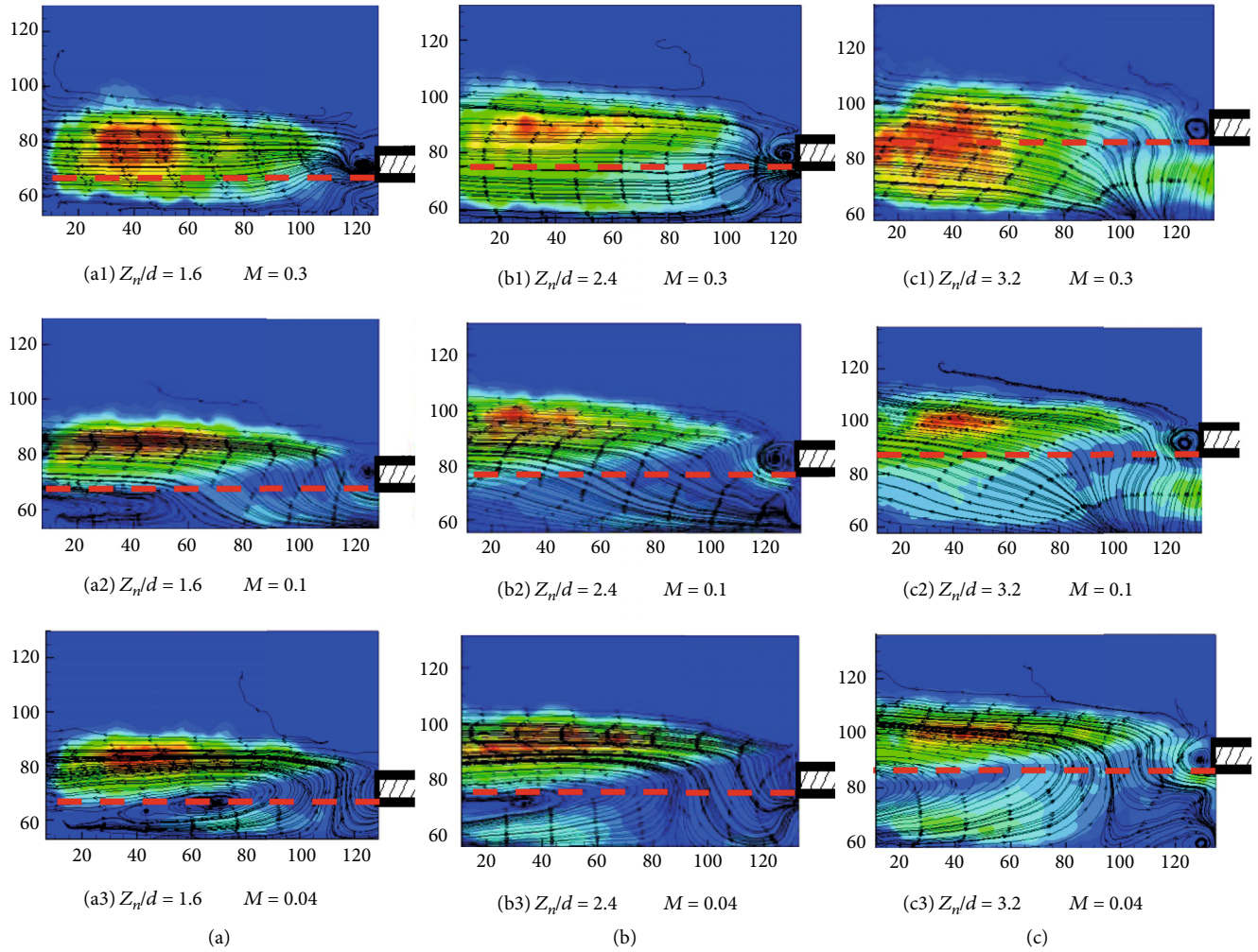

Figure 10: Flow field pattern at different jet-to-plate pitches.

beginning of the boundary between the shear layer and the primary hot airflow. It entrains the primary hot airflow into the shear layer, which makes the mixing stronger and the temperature of the airflow in the shear layer rise.

As the blowing ratio increases, the near-wall entrained vortex gradually moves downstream until it disappears in the interrogation area. This is because when the primary hot airflow mass flow rate and temperature are constant, the velocity and momentum of the secondary cold airflow in the slit outlet increase as the blowing ratio increases, and the separation of the downstream air flow decreases, so the vortex moves downstream. The blowing ratio increases, and the small vortex at the end of the inducting slab gradually becomes stronger. When the blowing ratio is increased, the speed of the slit outlet increases so that the reverse pressure gradient at the end of the inducting slab and the slit outlet further increases. Therefore, the strength of the small vortex increases with the increase of the blowing ratio, and the strength of the small vortex increases the primary hot airflow, and shear layer mixing is enhanced. This results in increased shear layer thickness. This makes the thickness of the film layer increases as the blowing ratio increases from 0.04 to 0.1. It can also be seen from the figure that when the blowing ratio is increased from 0.1 to 0.3, the thickness of the film layer slightly decreases because the disappearance of the separation zone downstream of the slit makes the overall film layer thinner.

In summary, as the blowing ratio increases from 0.04 to 0.3, the near-wall entrained vortex moves downstream, which reduces the primary hot airflow being drawn into the film plate wall, and the cold air covers the wall better. On the other hand, the vortex at the end of the inducting slab is stronger. This makes the mixing of the shear layer with the primary hot airflow stronger and increases the thickness of the shear layer.

3.2. Effect of the Temperature Ratio, T_R. Figure 9 shows how the flow field pattern changes with temperature ratios. Experiments were conducted by fixing the jet-to-plate pitch at 2.4, the spacing of impinging holes at 3.5, and the blowing ratios are 0.04, 0.1, and 0.3. The temperature ratios were then fixed at 0.73, 0.82, and 0.91, respectively.

At any blow ratio, the temperature ratio is increased by keeping the secondary cold airflow temperature constant and lowering the primary hot airflow temperature. The temperature ratio increases from 0.73 to 0.9 as the primary hot

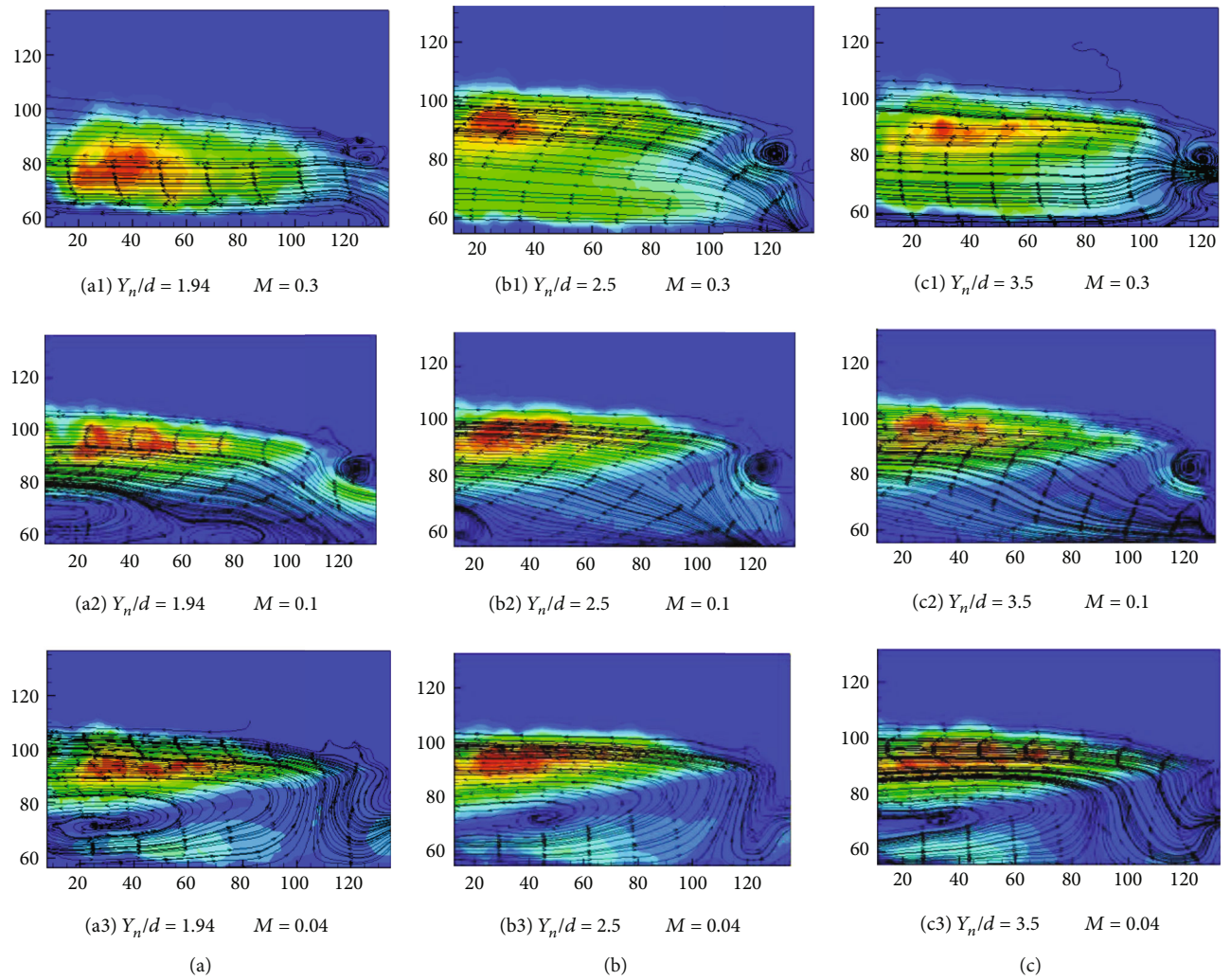

Figure 11: Flow field pattern at different spacing of impinging holes.

airflow temperature decreases from 423 K to 340 K. It can be seen from the figure that when the blowing ratio is 0.04, the radial size of the near-wall entrained vortex tends to decrease with the increase of temperature ratios. This is because of the decrease of the primary hot airflow velocity and the smaller entrainment effect on the downstream of the slit, which reduces the separation zone. When the blowing ratio is 0.1 and 0.3, the flow field pattern is basically similar as the temperature ratio increases.

3.3. Effect of Jet-to-Plate Pitch, Z_n. Figure 10 shows how the flow field pattern changes with jet-to-plate pitches. Experiments were conducted by fixing the temperature ratio at 0.73, the spacing of impinging hole 3.5, and the blowing ratios are 0.04, 0.1, and 0.3. The jet-to-plate pitches were then fixed at 1.6, 2.4, and 3.2, respectively. In the experiment, the diameter of the impinging hole was kept constant, and the jet-to-plate pitch was increased by increasing the distance between the film plate and the inducting slab. It can be seen from the figure that with the increase of the jet-to-plate pitch, the thickness in the radial direction of the development boundary of the film layer increases, but the shear height (the height of the film layer above the red line in Figure 8) does not change significantly. When the blowing ratio is 0.3, the secondary coolant airflow streamline changes from parallel wall to separation from the wall as the jet-to-plate pitch increases, and the effect of cooling gas covering the wall becomes worse. When the blowing ratio is 0.04 and 0.1, there is a near-wall entrained vortex downstream of the slit. As the jet-to-plate pitch increases, the location of the vortex center moves downstream, and the size of the vortex increases at the same time. This is because the larger the jet-to-plate pitch, the larger the area where the reverse pressure gradient is generated downstream of the slit. In summary, more cooling air needs to be consumed as jet-to-plate pitch increases under the condition of the same blowing ratio. At the same time, the size of the entrained vortex downstream of the slit outlet increases, and the near-wall airflow is severely separated. In engineering design, large jet-to-plate pitch should be avoided.

3.4. Effect of Spacing of Impinging Holes, Y_n. Figure 11 shows how the flow field pattern changes with spacing of impinging holes. Experiments were conducted by fixing the temperature ratio at 0.73, the jet-to-plate pitch at 1.6, and the blowing

ratios which are 0.04, 0.1, and 0.3. The spacing of impinging holes was then fixed at 1.94, 2.5, and 3.5, respectively. It can be seen from the figure that with the increase of the spacing of the impinging hole, the thickness in the radial direction of the development boundary of the film layer increases. When the blowing ratio is 0.04 and 0.1, there is a near-wall entrained vortex downstream of the slit, which moves downstream as the spacing of impinging hole increases. This is mainly because the diameter of the impact hole remains constant. When the spacing of the impinging hole increases, the number of impinging hole decreases, and the amount of secondary coolant airflow is constant. This results in an increase in the speed of the hole and a decrease in the uniformity of the velocity of the airflow in the slit. The exit speed of the downstream slit facing the hole is higher, and the exit speed of the downstream slit between the two holes is lower. In the experiment, the measured cross-section is a via-hole section. The increase in spacing of the impinging hole increases the local blowing ratio of the section. Therefore, the entrained vortex at the slit exit moves downstream. The vortex of the end of the inducting slab is strengthened, and the thickness of the shear layer is increased.

4. Conclusion

This paper focuses on the flow field characteristics of the impinging-film cooling under different geometric and flow conditions. The influence of each variable on the flow field characteristics is analyzed. Within the parameters of the experimental study, the conclusion is as follows:

(1) As the blowing ratio increases from 0.04 to 0.3, the near-wall entrained vortex moves downstream, which reduces the primary hot airflow being drawn into the film plate wall, and the cold air covers the wall better. On the other hand, the vortex at the end of the inducting slab is stronger. This makes the mixing of the shear layer with the primary hot airflow stronger and increases the thickness of the shear layer

(2) The radial size of the near-wall entrained vortex tends to decrease with the increase of temperature ratios when the blowing ratio is 0.04. This is because of the decrease of the primary hot airflow velocity and the smaller entrainment effect on the downstream of the slit, which reduces the separation zone. When the blowing ratio is 0.1 and 0.3, the flow field pattern is basically similar as the temperature ratio increases

(3) More cooling air needs to be consumed as jet-to-plate pitch increases under the condition of the same blowing ratio. The size of the entrained vortex downstream of the slit outlet increases, and the near-wall airflow is severely separated, and the effect of cooling gas covering the wall becomes worse

(4) As the spacing of the impinging hole increases, the local blowing ratio of the via-hole section increases. The entrained vortex at the slit exit moves downstream. The vortex of the end of the inducting slab is strengthened, and the thickness of the shear layer is increased. For the span section of the slit exit, the larger the spacing of the impact holes, the more uneven the velocity distribution of the air film

Data Availability

Some or all data, models generated, or used during the study are proprietary or confidential in nature and may only be provided with restrictions (e.g., model structure size).

Conflicts of Interest

We declare that we have no known competing financial interests or personal relationships with other people or organizations that can inappropriately influence our work.

Acknowledgments

This work was supported by the National Science and Technology Major Project [2017-Ill-0008-0034].

References

[1] D. G. Wilson and T. Korakianitis, *The Design of High-Efficiency Turbomachinery and Gas Turbines*, MIT press, 2014.

[2] A. H. Lefebvre and D. R. Ballal, *Gas Turbine Combustion*, Taylor & Francis Group, 3rd edition, 2010.

[3] Z. Q. Yu, C. Li, B. T. An, J. J. Liu, and G. Y. Xu, "Experimental investigation of film cooling effectiveness on a gas turbine blade pressure surface with diffusion slot holes," *Applied Thermal Engineering*, vol. 168, p. 114851, 2020.

[4] J. X. Yao, P. Su, J. He, J. Wu, J. Lei, and Y. Fang, "Experimental and numerical investigations on double-jet film-cooling with different mainstream incidence angles," *Applied Thermal Engineering*, vol. 166, p. 114737, 2020.

[5] S. D. Barahate and R. P. Vedula, "Film cooling performance measurement over a flat plate for a single row of holes embedded in an inclined trench," *International Journal of Thermal Sciences*, vol. 150, p. 106215, 2020.

[6] K. Qian, J. H. Wang, F. He, Y. D. Wu, and Z. H. Zhou, "An experimental investigation on transpiration cooling performances using solid hydrogel as coolant," *Applied Thermal Engineering*, vol. 158, p. 113753, 2019.

[7] G. Huang, Z. Y. Liao, R. N. Xu, Y. H. Zhu, and P. X. Jiang, "Self-pumping transpiration cooling with phase change for sintered porous plates," *Applied Thermal Engineering*, vol. 159, p. 113870, 2019.

[8] H. Su, F. He, J. H. Wang, N. Wu, R. Yao, and H. T. Han, "Numerical investigation on the characteristics of coolant flow, heat absorption and phase change in transpiration cooling process," *International Journal of Thermal Sciences*, vol. 142, pp. 68–76, 2019.

[9] K. Wang, H. Li, and J. Zhu, "Experimental study of heat transfer characteristic on jet impingement cooling with film extraction flow," *Applied Thermal Engineering*, vol. 70, no. 1, pp. 620–629, 2014.

[10] J. Wei, J. Zhang, S. Li, and F. Wang, "Numerical study on impinging-film hybrid cooling effect with different

geometries," *International Journal of Thermal Sciences*, vol. 92, pp. 199–216, 2015.

[11] J. Zhang, C. Yuan, P. Ji, J. Wei, and X. He, "Experimental investigation on the overall cooling effectiveness of t-type impinging-film cooling," *Applied Thermal Engineering*, vol. 128, pp. 595–603, 2018.

[12] J. ZHANG, S. ZHANG, C. WANG, and X. TAN, "Recent advances in film cooling enhancement: a review," *Chinese Journal of Aeronautics*, vol. 33, no. 4, pp. 1119–1136, 2020.

[13] Y. Q. Liu, P. X. Jiang, Y. B. Xiong, and Y. P. Wang, "Experimental and numerical investigation of transpiration cooling for sintered porous flat plates," *Applied Thermal Engineering*, vol. 50, no. 1, pp. 997–1007, 2013.

[14] A. Immarigeon and I. Hassan, "An advanced impingement/-film cooling scheme for gas turbines- numerical study," *International Journal of Numerical Methods for Heat & Fluid Flow*, vol. 16, no. 4, pp. 470–493, 2006.

[15] D. Singh, B. Premachandran, and S. Kohli, "Experimental and numerical investigation of jet impingement cooling of a circular cylinder," *International Journal of Heat and Mass Transfer*, vol. 60, pp. 672–688, 2013.

[16] S. Fechter, A. Terzis, P. Ott, B. Weigand, J. von Wolfersdorf, and M. Cochet, "Experimental and numerical investigation of narrow impingement cooling channels," *International Journal of Heat and Mass Transfer*, vol. 67, pp. 1208–1219, 2013.

[17] J. Ortega-Casanova and F. J. Granados-Ortiz, "Numerical simulation of the heat transfer from a heated plate with surface variations to an impinging jet," *International Journal of Heat and Mass Transfer*, vol. 76, pp. 128–143, 2014.

[18] R. Jia, B. Sunden, P. Miron, and B. Leger, "A numerical and experimental investigation of the slot film-cooling jet with various angles," *Heat Transfer*, vol. 127, pp. 845–856, 2008.

[19] T. Wang, S. Chintalapati, R. S. Bunker, and C. P. Lee, "Jet mixing in a slot," *Experimental Thermal and Fluid Science*, vol. 22, no. 1-2, pp. 1–17, 2000.

[20] C. A. Cruz, *Experimental and Numerical Characterization of Turbulent Slot Film Cooling*, Maryland University, 2008.

[21] S. Gogineni, D. Sutkus, and L. Goss, *Investigation of a Jet in a Cross Flow Using PIV*, Aerospace Sciences Meeting and Exhibit, 2013.

[22] F. Muldoon and S. Acharya, "DNS study of pulsed film cooling for enhanced cooling effectiveness," *International Journal of Heat and Mass Transfer*, vol. 52, no. 13-14, pp. 3118–3127, 2009.

[23] R. Hou, F. B. Wen, S. T. Wang, Y. X. Luo, and X. L. Tang, "Large eddy simulation of the trenched film cooling hole with different compound angles and coolant inflow orientation effects," *Applied Thermal Engineering*, vol. 163, p. 114397, 2019.

[24] F. Wu, L. Li, J. F. Wang, X. J. Fan, and C. H. Du, "Numerical investigations on flow and heat transfer of swirl and impingement composite cooling structures of turbine blade leading edge," *International Journal of Heat and Mass Transfer*, vol. 144, p. 118625, 2019.

[25] Y. Liu, Y. Rao, and L. Yang, "Numerical simulations of a double-wall cooling with internal jet impingement and external hexagonal arrangement of film cooling holes," *International Journal of Thermal Sciences*, vol. 153, p. 106337, 2020.

[26] A. Zamiri, S. J. You, and J. T. Chung, "Large eddy simulation of unsteady turbulent flow structures and film-cooling effectiveness in a laidback fan-shaped hole," *Aerospace Science and Technology*, vol. 100, p. 105793, 2020.